Cell**Press**

The CDC42-Interacting Protein 4 Controls Epithelial Cell Cohesion and Tumor Dissemination

Yannève Rolland,[1,6] Paola Marighetti,[1,6] Chiara Malinverno,[1] Stefano Confalonieri,[1,2] Chiara Luise,[1,2] Nadia Ducano,[3] Andrea Palamidessi,[1] Sara Bisi,[1] Hiroaki Kajiho,[1] Flavia Troglio,[1,2] Olga G. Shcherbakova,[5] Alexander R. Dunn,[5] Amanda Oldani,[1] Letizia Lanzetti,[3] Pier Paolo Di Fiore,[1,2,4] Andrea Disanza,[1,*] and Giorgio Scita[1,4,*]

[1]IFOM, Fondazione Istituto FIRC di Oncologia Molecolare, Via Adamello 16, 20139 Milan, Italy
[2]Dipartimento di Oncologia Sperimentale, Istituto Europeo di Oncologia, 20141 Milan, Italy
[3]Dipartimento di Scienze Oncologiche, Università degli Studi di Torino, Istituto per la Ricerca e la Cura del Cancro, Strada Provinciale 142 10060 Candiolo, Turin, Italy
[4]Dipartimento di Scienze della Salute, San Paolo, Università degli Studi di Milano, 20122 Milan, Italy
[5]Department of Chemical Engineering, Stanford University, Stanford, CA 94305, USA
[6]Co-first author
*Correspondence: andrea.disanza@ifom.eu (A.D.), giorgio.scita@ifom.eu (G.S.)
http://dx.doi.org/10.1016/j.devcel.2014.08.006

SUMMARY

The role of endocytic proteins and the molecular mechanisms underlying epithelial cell cohesion and tumor dissemination are not well understood. Here, we report that the endocytic F-BAR-containing CDC42-interacting protein 4 (CIP4) is required for ERBB2- and TGF-β1-induced cell scattering, breast cancer (BC) cell motility and invasion into 3D matrices, and conversion from ductal breast carcinoma in situ to invasive carcinoma in mouse xenograft models. CIP4 promotes the formation of an E-cadherin-CIP4-SRC complex that controls SRC activation, E-cadherin endocytosis, and localized phosphorylation of the myosin light chain kinase, thereby impinging on the actomyosin contractility required to generate tangential forces to break cell-cell junctions. CIP4 is upregulated in ERBB2-positive human BC, correlates with increased distant metastasis, and is an independent predictor of poor disease outcome in subsets of BC patients. Thus, it critically controls cell-cell cohesion and is required for the acquisition of an invasive phenotype in breast tumors.

INTRODUCTION

Epithelial cells organize into polarized, coherent sheets of cells, kept together by cell-cell adhesion structures. A key component of epithelial junctions in vertebrates is the transmembrane protein E-cadherin, which defines the so-called adherens junction (AJ) (Hyafil et al., 1981). AJs undergo rapid assembly and disassembly to enable epithelial tissue morphogenesis and rearrangement, as well as the acquisition of cell motility during epithelial-mesenchymal transition (EMT) (Thiery et al., 2009). However, how cell-cell adhesion is disrupted during EMT is poorly under-

stood. The key event in this process is the loss of E-cadherin-mediated cell-cell adhesion, most likely as a consequence of reduced E-cadherin transcription, although alternative mechanisms might exist.

A wealth of recent evidence points to a crucial role of E-cadherin endocytosis and recycling in tissue morphogenesis and EMT (Baum and Georgiou, 2011). Endocytic removal of E-cadherin from the cell surface is acutely induced by activation of receptor (Orlichenko et al., 2009) and nonreceptor (Avizienyte et al., 2002) tyrosine kinases, as well as by stimulation with transforming growth factor-β (TGF-β) (Janda et al., 2006). In the case of epidermal growth factor (EGF)-induced E-cadherin down-regulation and AJ disassembly, SRC has an important role. SRC forms complexes with E-cadherin and the EGF receptor (EGFR) (Shen et al., 2008) and, on activation, promotes EMT by phosphorylating E-cadherin and triggering its ubiquitination-dependent endocytosis and degradation (Fujita et al., 2002). Cell-cell adhesion can, in turn, modulate growth factor signaling (Qian et al., 2004), suggesting that E-cadherin endocytosis and signal transduction from receptor tyrosine kinases (RTKs) are intimately intertwined in the maintenance of epithelial cell morphogenesis, as well as in controlling epithelial cell motility. It remains unclear, however, how RTK activation induces E-cadherin dynamics and trafficking, what the key molecular determinants underlying this process are, and how E-cadherin endocytic machinery affects junctional tension.

One set of proteins ideally positioned to control E-cadherin trafficking and junctional stability are the FCH-Bin-Amphiphysin-Rvs (F-BAR)-domain containing proteins. In mammals, F-BAR proteins (hereinafter referred to as the TOCA family) include three members: TOCA-1 (Transducer of CDC42-dependent actin assembly), CIP4 (CDC42-interacting protein 4), and FBP17 (formin-binding protein 17). These proteins are implicated in clathrin-mediated endocytosis (CME), during which they sense and promote membrane curvature through their F-BAR domain and bind to key regulators of actin dynamics (e.g., the nucleation promoting factor N-WASP) and endocytosis (e.g., dynamin) through their SH3 domain (Itoh et al., 2005; Tian et al., 2000). Furthermore, TOCA-1 and CIP4 act as effectors of the

CrossMark

small GTPase CDC42 (Aspenström, 2009). Recently, both in *C. elegans* and in *Drosophila*, TOCA family proteins have been shown to localize at cell-cell junctions where they regulate cortical F-actin organization and junctional proteins (Georgiou et al., 2008; Giuliani et al., 2009; Leibfried et al., 2008). However, the functional role of this protein family in mammalian epithelial cell morphogenesis and epithelial tumor cell dissemination is unknown.

Here, we show that CIP4, by regulating E-cadherin internalization and junctional actomyosin contractility, controls cell scattering, EMT, and invasion in response to various motogenic signals. We further show that elevated CIP4 expression is selected in ERBB2+ and triple negative breast cancer (BC) tumors and correlates with increased risk of distant metastasis. Consistently, CIP4 is required for the conversion from ductal carcinoma in situ (DCIS) to invasive ductal carcinoma (IDC) in mouse xenograft models.

RESULTS

CIP4 Controls MCF10A Cell Cohesion

To investigate the hypothesis that the TOCA family proteins are involved in epithelial morphogenesis also in mammals, we silenced each of the members of the family in normal human mammary epithelial cells MCF10A, either individually or in combination (Figure 1A). CIP4-depleted cells—but not scramble-control (scr-CTR), TOCA1-knockdown (TOCA1-KD), or FBP17-KD cells— tended to cluster into cohesive colonies despite the presence of EGF, which is required for MCF10A growth and normally induces a scattered cell phenotype (Debnath et al., 2003) (Figure 1B). CIP4 removal significantly increased the number of tightly compacted colonies and concomitantly reduced the number of single isolated cells (Figure 1C). Simultaneous silencing of two or all three TOCA family proteins did not augment the proportion of compact colonies versus single cells observed following depletion of CIP4 alone (Figure 1C; Figure S1A available online). Furthermore, reconstitution of CIP4 in CIP4-KD cells, using an RNAi-resistant green fluorescent protein (GFP)-CIP4 expressed at levels comparable to the endogenous protein, restored a scattered cell phenotype, with significantly fewer and less compact cell clusters than in CIP4-KD cultures (Figures 1D–1F). Thus, removal of CIP4, but not of other TOCA family members, enhances cell cohesion and the formation of tightly adherent cell clusters.

Next, we investigated cell-cell junction status after CIP4 removal, focusing on AJs. CIP4 depletion caused a marked increase in junctional E-cadherin in clustered cells as compared to scramble-control (scr-CTR) cells (Figures S1B and S1C), without affecting the rate of cell proliferation (Figure S1D). The formation of compact colonies following CIP4 removal was also accompanied by a homogenous distribution of the Golgi complex that was oriented in the majority of clustered CIP4-KD cells (>70%) toward the free-facing surface of the cell (Figure S1E). In contrast, control cells formed loosely adherent colonies, which displayed a randomly oriented Golgi complex, even in cells engaged in junctional contacts along three sides (compare insets in Figure S1E). Additionally, CIP4-KD cell colonies displayed thick F-actin cables along the external cortex, while F-actin was reduced along cell-cell junctions as compared

to scr-CTR or TOCA-1-KD and FBP17-KD cells (Figure S1F). Collectively, these findings indicate that CIP4 is unique among the TOCA family members in that it regulates cell cohesion and junctional adhesion of MCF10A cells.

CIP4 Does Not Influence Motility Parameters of Individual MCF10A Cells but Indirectly Controls the Motility Behavior

The dynamic remodeling of cell-cell junctions is crucial for epithelial cell motility. Thus, we tested the motility of the different MCF10A TOCA family-KD cells. In the presence of EGF, control cells were scattered and highly motile. In contrast, CIP4-KD cells tended to aggregate into clusters and ceased migration (Movie S1). Indeed, quantification of motility parameters indicated that CIP4-KD cells displayed markedly reduced velocity once they encountered a cell cluster (Figure S2A). However, isolated CIP4-KD cells moved at a speed similar to that of control cells (Figure S2B), arguing that CIP4 has no major effect on the basic cell locomotion machinery. Similar migratory behavior was observed in the 2KD and 3KD cells (Figures S2A and S2B), whereas, TOCA1-KD and FBP17-KD MCF10A cells resembled control cells, albeit removal of FBP17 reduced slightly cell velocity (Figures S2A and S2B and Movie S1). Notably, all cell lines eventually formed an epithelial monolayer and established stable cell-cell junctions. Additionally, the ability of MCF10A cells to migrate into a wound as a cohesive cohort was not affected by removal of CIP4 (Figure S2C). Together, these results suggest that CIP4 indirectly controls motility behavior, likely by stabilizing AJs.

CIP4 Is Required for EGF-Induced Scattering of MCF10A Cells but Does Not Affect EGFR Signaling, EGFR Trafficking, and CDC42-N-WASP Activation

In the presence of EGF, control MCF10A cells, seeded sparsely, were scattered, elongated, and failed to form stable cell-cell contacts (Figure S2D). After EGF deprivation, control cells, TOCA1-KD, and FBP17-KD cells, formed compact cell clusters similarly to CIP4-KD cells grown in the presence of EGF (Figures S2D and S2E). These results suggest that CIP4-KD cells might be defective in responding to acute EGF stimulation. To test this possibility, we performed EGF-induced cell scattering assays. Control and CIP4-KD cells deprived of EGF form compact clusters. On EGF stimulation, control cells became very motile and were almost completely scattered 2 hr after EGF addition (Movie S2). In contrast, CIP4-KD cells were immobile and did not start to scatter until 11 hr after EGF stimulation (Figure 1G and Movie S2). We further quantified cell scattering by measuring the total distance traveled by cells from their original position within a colony. Removal of CIP4 reduced the scattering distance by ~80% compared to control cells (Figure 1H). The increased cell compaction and delayed scattering of CIP4-KD cells suggests that CIP4 might affect the ability of epithelial cells to invade into the extracellular matrix (ECM). Consistently, CIP4 removal significantly impaired the invasive, EGF-dependent chemotaxis of MCF10A cells into Matrigel-coated transwells (Figure 1I).

To determine whether defective EGF-induced cell scattering of CIP4-KD cells was due to alterations in EGFR signaling or trafficking, we first evaluated the levels of EGFR expression.
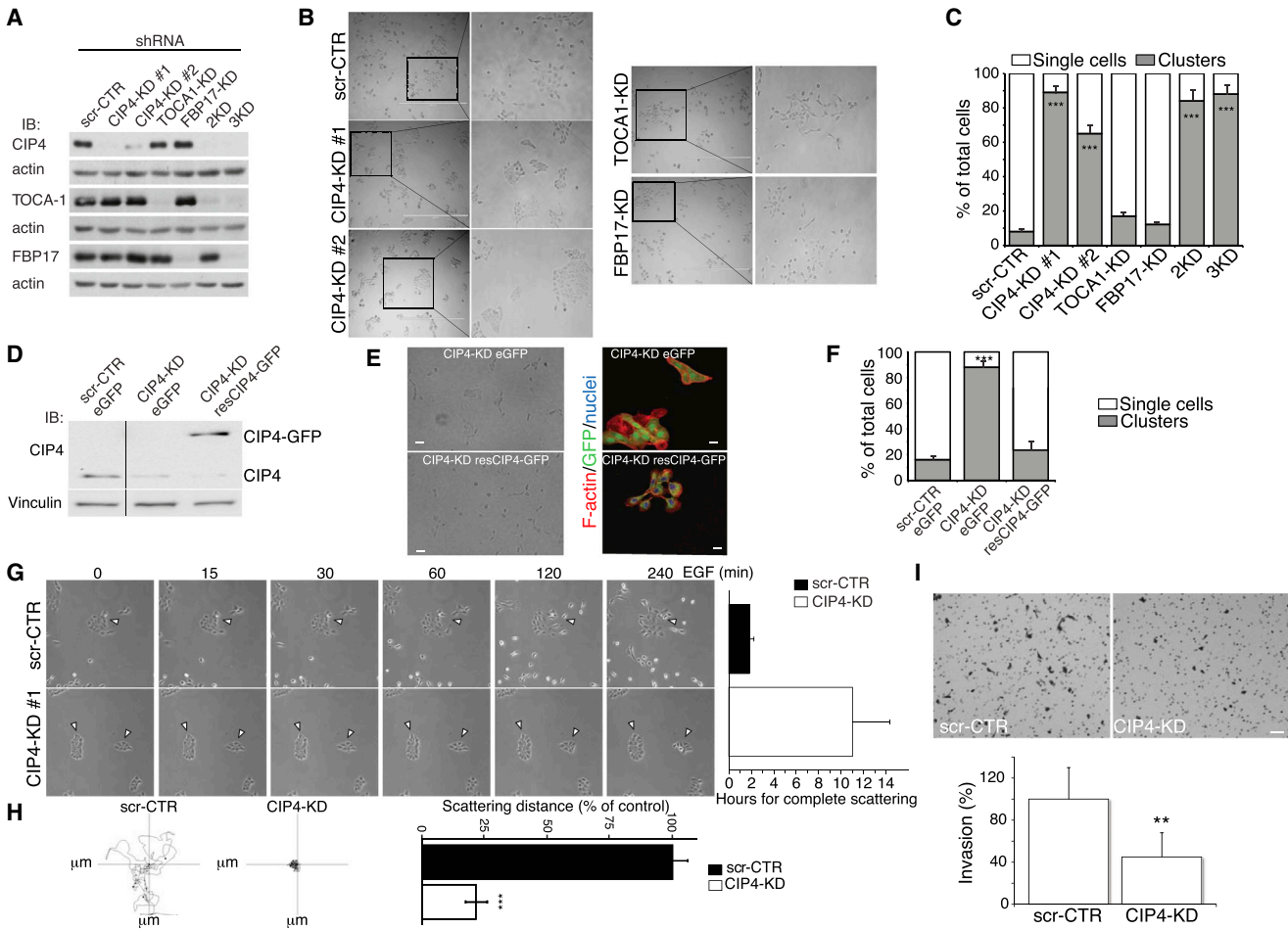
Figure 1. CIP4 Regulates MCF10A Cell Compaction and EGF-Induced Scattering

(A) IB with indicated antibodies of lysates of shRNA-lentivirally infected MCF10A cells: scr-CTR and shRNAs against CIP4 (CIP4-KD #1 and #2), TOCA-1 (TOCA1-KD), or FBP17 (FBP17-KD), alone or together (CIP4/TOCA-1 double KD; 2KD) (CIP4/TOCA-1/FBP17 triple KD; 3KD).

(B) Phase contrast images of various MCF10A cell lines growing in complete medium. Magnified view of the boxed area is shown. Scale bars represent 1,000 μm.

(C) The percentage of single cells or clusters relative to the scr-CTR MCF10A cells (n = 200 cells per genotype in three independent experiments). ***p < 0.001, t test.

(D) Expression levels of CIP4 by IB in scr-CTR and CIP4-KD MCF10A cells expressing an shRNA-resistant CIP4 mutant (resCIP4-GFP) or an empty GFP vector (eGFP).

(E) Images of CIP4-KD#1 MCF10A cells expressing GFP or resCIP4-GFP. Left panels: low magnification of GFP- or resCIP4-expressing CIP4-KD. Scale bar represents 100 μm. Right panels: merged images of GFP epifluorescence (green), F-actin (red), and DAPI nuclei (blue). Scale bar represents 20 μm.

(F) The number of single and clustered cells was quantified as in (C) (n = 226–647 cells). ***p < 0.001, t test.

(G and H) Still images of scr-CTR and CIP4-KD#1 MCF10A cells induced to scatter by adding EGF (100 ng/ml) to EGF-starved cells. Cell scattering quantified either (right graph) (G) by determining the time required to complete scattering or (H) by tracking individual cells, measuring accumulated distance covered by cells during 4 hr after EGF stimulation. Data indicate the percentage of accumulated scattering cell distance with respect to control cells (n = 25 cells per experiment in four experiments). ***p < 0.001, t test.

(I) Invasion through Matrigel-coated transwells toward EGF assessed for 24 hr. Representative images are shown. Cell invasion is the percentage of invasive cells with respect to control cells. **p < 0.01, t test.

Error bars indicate mean ± SEM. See also Movie S2.

We detected no significant differences in total or cell surface levels of EGFR among the cell lines tested (Figures S3A and S3B). Similarly, CIP4 depletion did not significantly alter EGFR signaling as determined by measuring the levels of activated ERK1/2, AKT (Figure S3C), and EGFR (Figure S3F).

TOCA family members have been shown to control early events of EGFR CME and trafficking (Itoh et al., 2005). However, CIP4 depletion did not significantly alter the rates of EGFR endo-cytosis (Figure S3D), recycling (Figures S3D and S3E), or the extent of EGFR degradation (Figure S3F). Thus, CIP4 is dispensable for EGFR signaling, stability, and intracellular trafficking.

TOCA family members are also essential for activation of N-WASP/WASP downstream of CDC42. However, removal of CIP4 did not alter EGF-mediated activation of N-WASP, monitored by measuring its tyrosine phosphorylation (Torres and Rosen, 2003) (Figure S3G), suggesting that this latter pathway
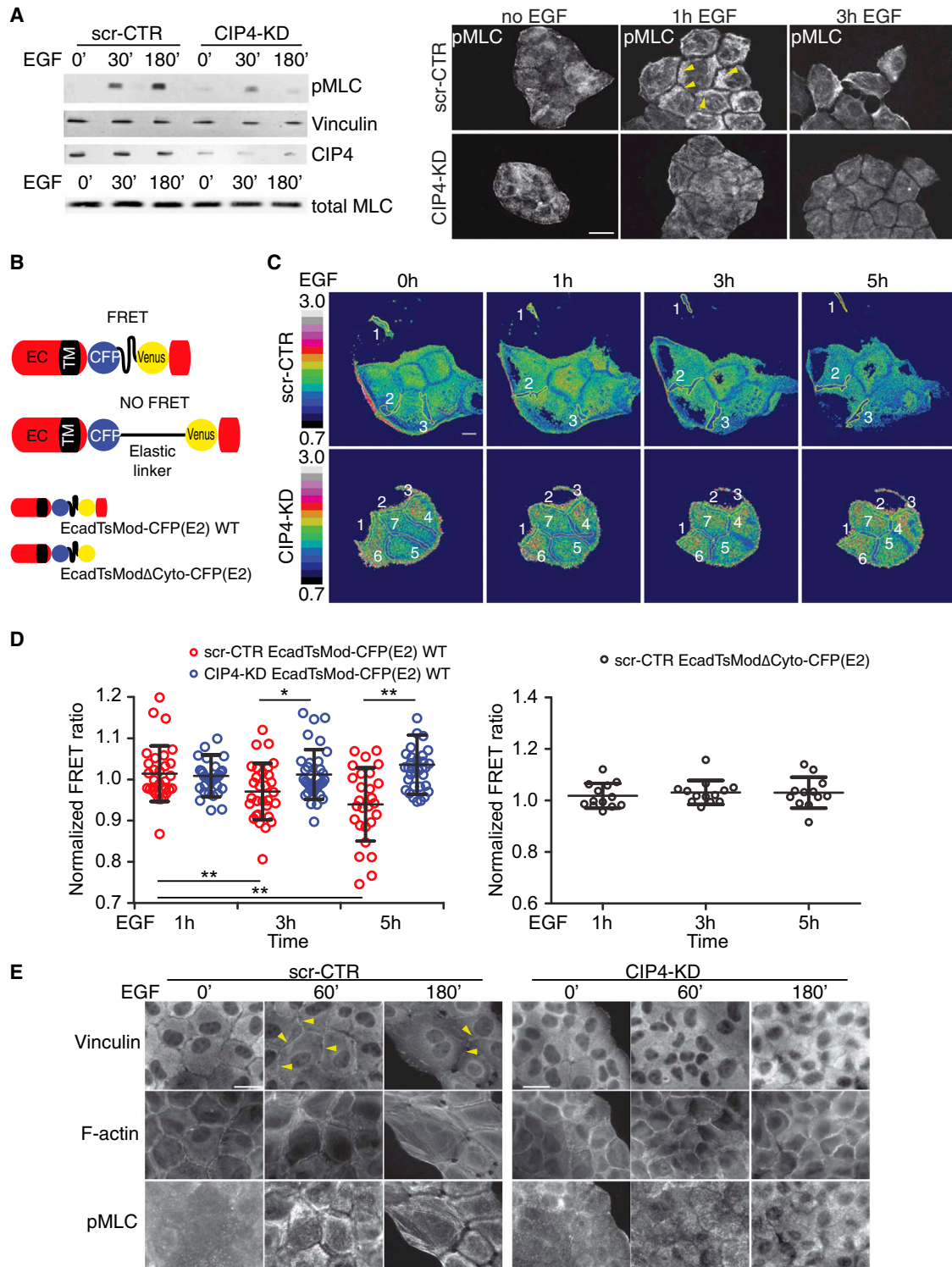
Figure 2. CIP4 Controls EGF-Induced Actomyosin Tensile Junctional Stress across E-cadherin

(A) Left panels: IB of lysates of scr-CTR and CIP4-KD MCF10A cells treated with EGF (100 ng/ml), antibodies as indicated. Right panels: EGF-deprived scr-CTR and CIP4-KD #1 MCF10A cells plated on plastic stimulated with EGF and stained with anti-pMLC antibodies or phalloidin to detect F-actin. Arrows indicate pMLC at junctions. Scale bar represents 25 μm. h, hours.

(B) Scheme of E-cadherin tensor sensor.

(C) Representative images from Movie S4 showing the FRET:CFP(E2) ratio of scr-CTR and CIP4-KD-MCF10A cells expressing the EcadTsMod-CFP and induced to scatter by EGF addition. The upper and lower limits of the FRET:CFP ratio range are shown on the left in the RATIO colored key (ImageJ software). CIP4-KD

is not responsible for the increased cell cohesion following CIP4 silencing.

CIP4 Controls Cell Scattering and Cohesion by Regulating EGF-Induced Actomyosin Contraction

Epithelial cell scattering depends on modulation of junctional-localized actomyosin contractility (de Rooij et al., 2005). Indeed, analysis of enhanced green fluorescent protein (EGFP)-E-cadherin dynamics during Madin-Darby canine kidney cell scattering revealed that tensile, orthogonal stresses build up along cell-cell junctions until cells are pulled apart (de Rooij et al., 2005). We observed a similar dynamic behavior of junctional EGFP-E-cadherin during EGF-mediated scattering of MCF10A cells (Movie S3). Conversely, in CIP4-depleted cells, orthogonal tensile stress was insufficient to pull apart cell-cell junctions (Movie S3). This result suggests that CIP4 might regulate EGF-dependent contractility at junctions. To test this possibility, we investigated the phosphorylation of the myosin II regulatory light chain (pMLC), the main regulatory event leading to actomyosin contractility (Bresnick, 1999). EGF stimulation increased total levels of pMLC and promoted the accumulation of pMLC adjacent to cell-cell junctions in control cells. Both these events were markedly diminished following CIP4 depletion (Figure 2A; Figure S4A). To verify that CIP4 removal causes cell compaction, at least in part, by impairing the localized accumulation of pMLC and, thus, actomyosin contractility, we performed three additional sets of experiments. In the first approach, we took advantage of the finding that junctional E-cadherins act as mechanosensor devices (Borghi et al., 2012). We used a next-generation Förster resonance energy transfer (FRET)-based, E-cadherin tension sensor [EcadTSMod-CFP(E2)] to measure the magnitude of tensile forces transmitted through the cytoplasmic domain of E-cadherin (Borghi et al., 2012). The EcadTSMod is built by inserting in the cytoplasmic tail of E-cadherin the monomeric, aggregation-free variant of CFP, CFP(E2), followed by a spider silk fragment that functions as a nanospring and Venus (A206K) (Borghi et al., 2012). Under conditions of low tension, CFP(E2) and Venus are close enough to undergo FRET; however, when orthogonal tensile force is applied, the distance between the two fluorescent proteins increases and FRET decreases (Figure 2B). Thus, the FRET signal responds to mechanical tension across the E-cadherin molecule. EcadTSMod_CFP(E2) is properly localized along the junction (Figure 2C). We also expressed an EcadTSModΔcyto-CFP(E2) as a control construct, which can no longer interact with the underlying actin cytoskeleton due to the lack of the β-catenin–binding domain; hence, it is insensitive to tensile stresses (Borghi et al., 2012). Under EGF deprivation, both scr-CTR and CIP4-KD cells display similar elevated E-cadherin FRET index at cell-cell junction. However, following EGF stimulation, the junctional FRET index significantly decreased in scr-CTR but not in CIP4-KD (Figures 2C and 2D; Movie S4). We detected no variation in the FRET in-

dex when EcadTSModΔcyto was used (Figure 2D). Thus, loss of CIP4 prevents the accumulation of tension across junctional E-cadherin. As a second approach, we exploited findings demonstrating that the mechanoresponse of E-cadherin is potentiated by vinculin, which is specifically recruited to anchor sites within AJs in a myosin II- and actomyosin contractility-dependent fashion (le Duc et al., 2010). Consistently, we found that, in control MCF10A cells, EGF induced accumulation of pMLC at adhesion sites, which was accompanied by the accumulation of vinculin (Figure 2E). Conversely, little or no detectable vinculin accumulated at cell-cell junctions after removal of CIP4, mirroring the lack of pMLC recruitment (Figure 2E). Third, we reasoned that we should be able to rescue defective EGF-induced accumulation of junctional pMLC and cell scattering in CIP4-KD cells by enhancing cell contractility. Actomyosin contractility is dependent on ECM cell adhesion (Geiger et al., 2009). Furthermore, increased cell adhesion strength correlates with increased cell scattering (de Rooij et al., 2005). Hence, we tested whether plating cells on an ECM that is known to activate integrin-mediated adhesion and actomyosin contractility rescued defective cell scattering of CIP4-KD cells. MCF10A cells rapidly adhere and spread when plated onto fibronectin (Fn) but poorly adhere to laminin and vitronectin (Figure S5A). CIP4 removal slightly delayed adhesion to Fn but did not affect cell spreading, integrin-dependent activation of focal adhesion kinase (FAK; Figures S5A–S5C) or the surface levels of total and active β1 and of total α5β1 integrins (Figure S5D), despite a reduction in the internalization of β1 adhesion receptors (Figure S5E). However, the cell scattering deficiency and cell cohesion of CIP4-KD cells were rescued by plating cells onto Fn (Figures 3A and 3B; Figures S4B–S4D; Movie S5). This correlated with increased EGF-induced levels of total and junctional-localized pMLC (Figure 3C and Figure S4B). Collectively, these results suggest that CIP4 is required to promote optimal EGF-induced actomyosin contractility, which contributes to the generation of sufficient tension to break cell junctions apart and promote cell scattering.

CIP4 Is Required for E-cadherin Internalization on EGF Stimulation

EGF stimulation promotes E-cadherin mobilization and disassembly (Shen et al., 2008). The increased cell cohesion resulting from CIP4 removal could partly be explained by a direct effect of CIP4-KD on E-cadherin expression. However, E-cadherin levels were not significantly different between control and CIP4-KD MCF10A cells (Figure 4A). Alternatively, CIP4 might influence E-cadherin trafficking. We first examined EGFP-E-cadherin dynamics after stimulation with EGF. Depletion of CIP4 impaired increased E-cadherin internalization induced by EGF (Figure 4B) and prevented junctional disruption (Figure 4B and Movie S3). Next, we quantified E-cadherin internalization using a surface biotinylation and internalization assay. Silencing of CIP4 (either alone or in conjunction with other TOCA family members)

cells appear smaller due to compaction. White numerals indicate examples of manually defined cell-cell junction areas used to measure the FRET:CFP ratio range of the EcadTsMod-CFP sensor. Scale bar represents 10 μm.

(D) Normalized FRET ratio at cell-cell junction of MCF10A cells treated as in (C). For each cell-cell contact, data were normalized to the FRET/CFP ratio value at time 0 hr. Data are expressed as mean ± SEM. (n = 30 cell-cell contacts/experiment from three experiments). *p < 0.05; **p < 0.01, t test.

(E) EGF-deprived scr-CTR and CIP4-KD#1 MCF10A cells plated on plastic were stimulated with EGF and stained with the anti-Vinculin antibodies or phalloidin to detect F-actin. Arrows indicate vinculin. Scale bar represents 20 μm.
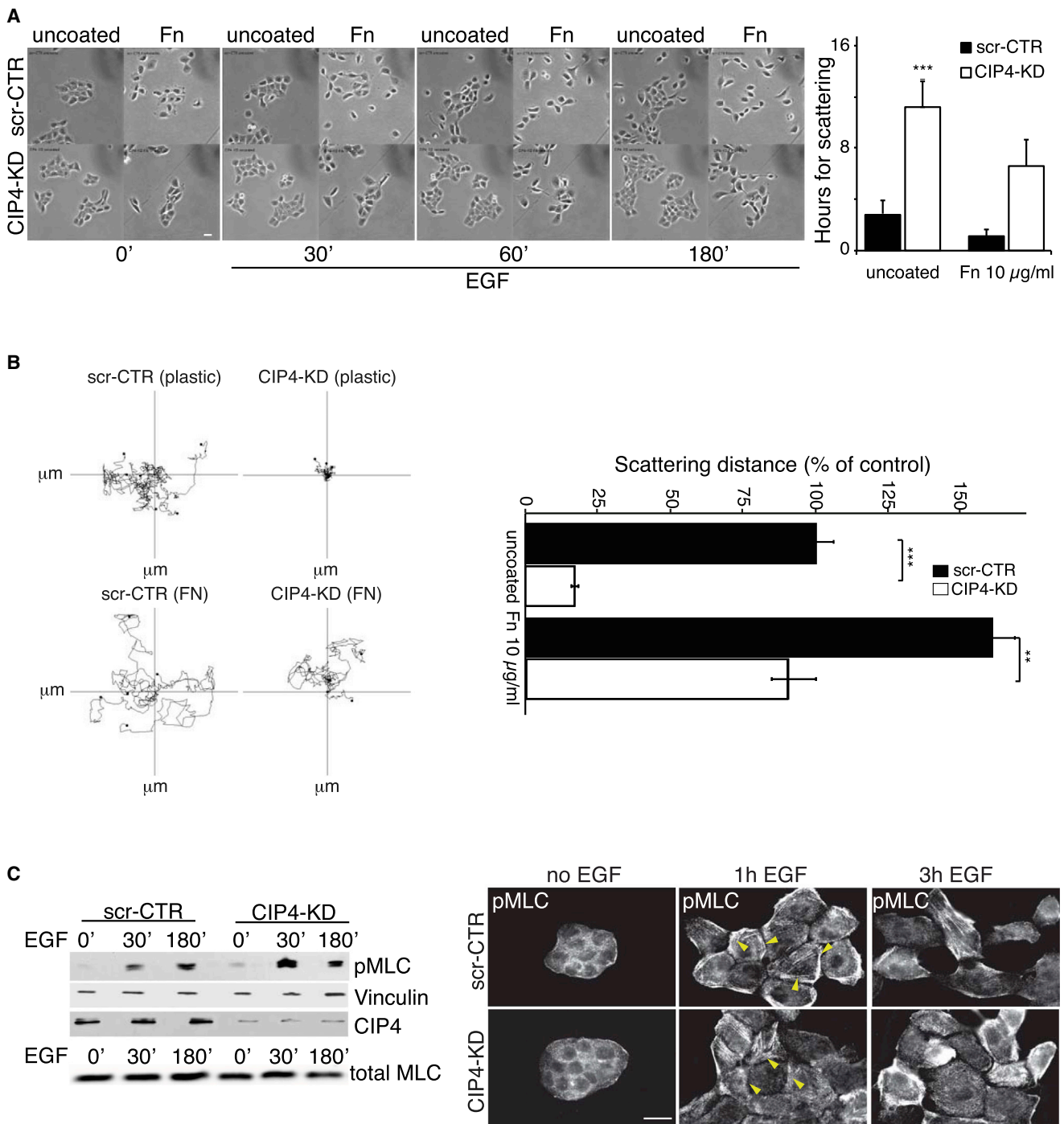
Figure 3. Fn Adhesion Rescues Delayed Scattering and Reduces Junctional Actomyosin Contractility

(A) Control and CIP4-KD MCF10A cells plated on plastic (uncoated) or Fn for 24 hr, EGF starved, and stimulated with EGF to induce scattering. Representative images are shown. Graph on the left represents the time to reach complete scattering (***p < 0.001, compared to scr-CTR cells). Error bars indicate mean ± SEM. Scale bar represents 20 μm.

(B) Cell scattering quantified as described in Figure 2D. Left: exemplar tracks of individual cells undergoing scattering. Right: the accumulated scattering distance is expressed as the percentage of scr-CTR (n = 25 per experiment, three experiments). Error bars indicate mean ± SEM. **p < 0.01, compared to scr-CTR MCF10A cells.

(C) Left panels: lysate of scr-CTR and CIP4-KD#1 MCF10A cells plated on Fn were subjected to IB for indicated antibodies. Right panels: EGF-deprived scr-CTR and CIP4-KD#1 MCF10A cells plated on Fn were stimulated with EGF and stained with the anti-pMLC antibodies or phalloidin to detect F-actin (see also Figure S4B). Arrows indicate pMLC at junctions. ***p < 0.01, compared to scr-CTR MCF10A cells. Scale bar represents 25 μm. h, hours.

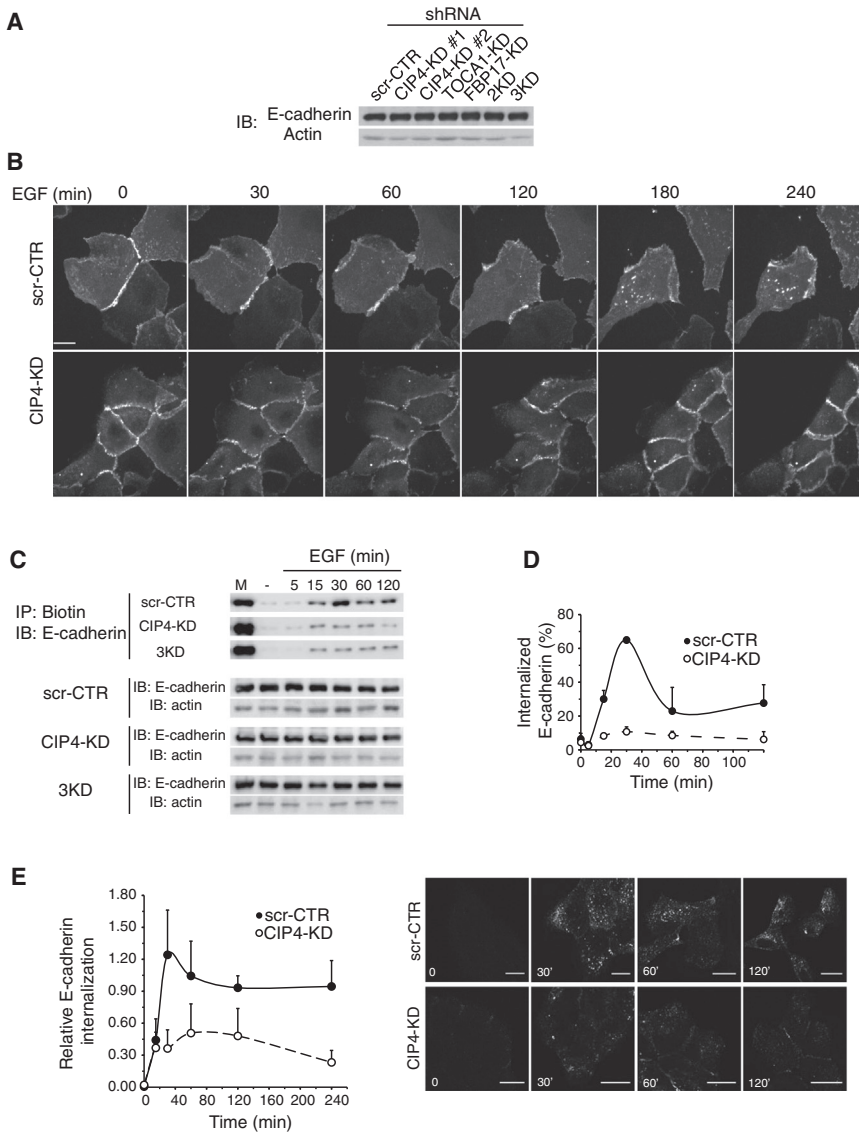**A**

B

C

D

E

Figure 4. CIP4 Is Required for the Internalization of E-cadherin on EGF Stimulation

(A) IB of lysates of scr-CTR or MCF10A cells devoid of TOCA family members and grown in complete medium to detect E-cadherin.

(B) Internalization of E-cadherin-GFP on acute EGF stimulation of EGF-starved MCF10A cells. Still images are from Movie S4. Scale bar represents 10 μm.

(C) Surface biotinylation of MCF10A cells. Internalization of E-cadherin on stimulation with EGF for up to 120 min at 37°C. Surface levels of biotinylated E-cadherin are shown for unstimulated cells maintained at 4°C (M, membrane) and after washing with MESNA buffer (−, negative control). IBs in the lower panel show E-cadherin and actin in cell lysates used to perform biotin pulldowns.

(D) Quantification of internalized E-cadherin from the biotinylation assay expressed as percentage of cell-surface E-cadherin levels (n = 3 experiments). Error bars indicate mean ± SEM.

(E) Internalization of surface-labeled E-cadherin using anti-E-cadherin (HECD-1) antibodies. Relative levels of internalized E-cadherin are quantified by evaluating total fluorescence intensity normalized for cell number and field area. Error bars indicate mean ± SEM. Scale bars represent 20 μm.

CIP4 Interacts with E-cadherin and SRC in MCF10A Cells after EGF Stimulation

To gain clues as to the molecular mechanisms underlying the role of CIP4 in EGF-dependent endocytosis of E-cadherin, we first assessed whether CIP4 intracellular localization was affected by EGF stimulation. CIP4 is primarily distributed in the cytoplasm in EGF-deprived MCF10A cells (Figure 5A). EGF stimulation promoted CIP4 relocalization to membrane ruffles (Figure 5A) and cell junctions, where it partially colocalized with E-cadherin, suggesting that the two proteins might associate in a growth-factor-dependent manner (Figure 5A). Consistently, CIP4 and E-cadherin coimmunoprecipitated, and this interaction was enhanced by stimulation with EGF (Figure 5B).

Another important regulator of E-cadherin signaling, trafficking, and actomyosin contractility is the non-RTK SRC (Andreeva et al., 2014; Avizienyte et al., 2002; Palacios et al., 2005). As previously shown (Canel et al., 2010), pharmacological inhibition of SRC family activity with PP2 or Dasatinib (Figure S6B) significantly impaired E-cadherin endocytosis (Figure S6C) and EGF-induced cell scattering (Figure S6D), both in control and CIP-KD cells. SRC has been shown to interact with and phosphorylate CIP4 (Dombrosky-Ferlan et al., 2003; Hu et al., 2011). Thus, we tested whether CIP4, in addition to interacting with E-cadherin, also interacts with SRC. We observed that endogenous SRC and CIP4 coimmunoprecipitated and that their interaction was enhanced by EGF stimulation (Figure 5B), suggesting that CIP4 enters into a complex with E-cadherin and SRC. Removal of CIP4 reduced the amount of

significantly decrease EGF-induced internalization of E-cadherin (Figures 4C and 4D).

To corroborate these latter observations, we also used HECD-1, an antibody that recognizes the extracellular domain of E-cadherin, to monitor EGF-induced internalization of E-cadherin (Figure 4E and Figure S6A). EGF induced a rapid internalization of E-cadherin, which was impaired by removal of CIP4. The extent and kinetics of E-cadherin endocytosis measured using the HECD-1 antibody were similar to those obtained using the biotinylation assay (compare Figure 4E with Figure 4D). Thus, CIP4 is required to promote EGF-induced E-cadherin endocytosis.

Collectively, our data indicate that CIP4 is a pivotal regulator of epithelial morphogenetic events that controls the amount of junctional E-cadherin through endocytosis and growth-factor-induced, cell-adhesion-dependent actomyosin contractility, thereby coordinating cell-cell adhesion in response to soluble stimuli.

Figure 5. EGF Induces Redistribution of CIP4 to Junctions and Its Interaction with E-cadherin and SRC in MCF10A Cells

(A) EGF-deprived MCF10A cells were stimulated with EGF for 5 min at 37°C, fixed, and stained to detect CIP4 (red) and either F-actin or E-cadherin (green). Insets are higher magnification of boxed areas. White arrows indicate peripheral and junctional plasma membrane. Scale bar represents 20 μm.

(B) MCF10A cells were EGF starved for 18 hr and mock treated (−) or stimulated with EGF (+) for 30 min at 37°C. Total cell lysates (1 mg) were immunoprecipitated with anti-CIP4 antibody or irrelevant immunoglobulin G (IgG). Total cell lysates (60 μg) and immunoprecipitates (IPs) were subjected to IB with the indicated antibodies.

(C) Lysates of control (scr-CTR) or CIP4-KD MCF10A cells, treated as in (B), were immunoprecipitated with anti-SRC antibody. IPs were subjected to IB with the indicated antibodies. Relative intensity of the phospho-SRC (p-SRC) signal with respect to total SRC is shown (n = 3).

(legend continued on next page)

E-cadherin coimmunoprecipitating with SRC on EGF stimulation and inhibited EGF-induced SRC activation (Figure 5C). Thus, CIP4 enters into and promotes the formation of an EGF-dependent E-cadherin/SRC complex and controls SRC activation. We further characterized the nature of the SRC/CIP4 interaction using in vitro binding experiments. We found that the SH3 domain of SRC was sufficient to pull down CIP4 (Figure 5D), and we identified a potential SH3 binding site of CIP4 encompassing amino acids 485–505. Deletion of the central P492 and P493 residues (ΔP-CIP4) reduced the binding of CIP4 to the SRC SH3 domain (Figure 5D). Notably, the interaction between the SRC SH3 domain and CIP4 was detectable only after stimulation with EGF, confirming coimmunoprecipitation experiments (Figure 5E). To demonstrate the functional relevance of the CIP4/SRC interaction, we reconstituted CIP4-KD cells either with small interfering RNA (siRNA)-resistant wild-type (WT)-CIP4 or ΔP-CIP4 mutant. Only the expression of WT-CIP4, but not of ΔP-CIP4, restored the cell compaction (data not shown) and scattering phenotypes (Figure 5F and Movie S6).

CIP4 Facilitates TGF-β1-Induced Mesenchymal Morphological Conversion of MCF10A Cells

Endocytosis of E-cadherin also occurs during TGF-β1-induced EMT (Janda et al., 2006). TGF-β1 promotes permanent loss of cell adhesion by negatively regulating E-cadherin expression and by modulating dynamin-dependent endocytosis (Ogata et al., 2007). We thus tested whether CIP4 is involved in TGF-β1-induced scattering and junctional remodeling. Depletion of CIP4 inhibited both of these TGF-β1-induced effects (Figure 6A). To assess whether CIP4 is required for activation of the TGF-β1-dependent transcriptional program that underlies EMT, we measured messenger RNA (mRNA) levels of the transcription factors, Snail1 and Snail2. The expression of these transcription factors was, as expected, regulated by TGF-β1, and CIP4 removal had only a marginal effect on (Snail2) or delayed (Snail1) expression (Figure 6B). Since TGF-β1 also controls E-cadherin expression and promotes an E-cadherin/N-cadherin switch (Peinado et al., 2004), we next determined the total levels of these junctional proteins. While removal of CIP4 did not affect E-cadherin levels, N-cadherin expression was reduced in untreated CIP4-KD cells compared to control cells (Figure 6B and 6C). However, stimulation with TGF-β1 increased N-cadherin expression in both cell types to a similar extent, further suggesting that CIP4 depletion does not affect TGF-β1 signaling (Figure 6C). We therefore assessed whether removal of CIP4 influences TGF-β1-induced E-cadherin endocytosis and found that this response was delayed in CIP4-KD cells (Figures 6E and 6F). Notably, TGF-β1 also caused a transient elevation of CIP4 mRNA that

was accompanied by an increase in CIP4 protein (Figures 6C and 6D), at a time coincident with the onset of cell scattering. CIP4 depletion was also accompanied by impaired TGF-β1-dependent SRC activation, which was short lived compared with controls, suggesting that the CIP4-SRC axis is also involved in TGF-β1-induced cell scattering (Figure 6G).

Finally, since EMT is invariably associated with increased migratory and invasive properties, we pretreated control and CIP4-KD cells with TGF-β1 and determined their invasive ability through Matrigel-coated transwells. Removal of CIP4 significantly impaired TGF-β1-induced invasion in both the presence and the absence of EGF (Figure 6H). This result corroborates the importance of CIP4 in the remodeling of junctional E-cadherin required for epithelial cell plasticity.

Deregulation of CIP4 in Human BC

The role of CIP4 in the control of cell cohesion and cell invasion suggests that invasive human BCs might positively select for elevated levels of this protein. To test this hypothesis, we analyzed by immunohistochemistry (IHC) formalin-fixed paraffin-embedded tissue microarrays (TMAs) of human BC using a specific anti-CIP4 antibody (Figure 7A; Figures S7A and S7B). The level of CIP4 was significantly increased in clinically aggressive, estrogen-receptor (ER)- and progesterone-receptor (PgR)-negative and ERBB2-positive BCs (Figure 7B), and its elevated expression was significantly associated with disease relapse. Notably, in ER- and PgR-positive tumors, as well as in ERBB2-negative tumors, which usually have a good prognosis, elevated expression of CIP4 was still significantly associated with disease recurrence (Figure 7C). Moreover, in grade 2 breast tumors, which are associated with an intermediate risk of recurrence, CIP4 overexpression was associated with poor outcome (Figure 7C). Multivariate analysis corroborated this finding revealing that CIP4 expression is an independent predictor of poor prognosis of disease relapse (Figure 7D). Although an analysis of a larger cohort of primary, and possibly metastatic, tumors is necessary to gain a complete picture of the clinical significance of CIP4 overexpression, our TMA analysis provides statistically significant evidence in support of our conclusion that CIP4 is positively associated with highly aggressive, metastatic, ERBB2-positive BCs.

CIP4 Is Required for ERBB2-Induced Invasive Outgrowth of Mammary Epithelial Cells and Conversion of Breast Ductal Carcinoma In Situ to Invasive Carcinoma

To test whether CIP4 is involved in promoting invasive behavior and local dissemination, we used various in vitro and in vivo

(D) Lysate of EGF-stimulated WT- or ΔP-CIP4-293T cells stimulated with EGF (100 ng/ml) incubated with glutathione S-transferase (GST)- or GST-SH3 domain-bound to bead of SRC. Input and bound material were immunoblotted with the anti-CIP4 antibody. As control, GST-SH3 beads were also incubated with lysate buffer alone (no lysate).

(E) EGF-deprived flag-tagged WT- or ΔP-CIP4-293T cells were stimulated with EGF for 30 min. Lysates were incubated with equimolar amounts of GST or GST-SH3 domain of SRC and immobilized on glutathione beads. Input and bound material were immunoblotted with the anti-CIP4 antibody.

(F) scr-CTR and CIP4-KD #1 MCF10A were lentivirally infected with either an empty vector or with vector encoding siRNA-resistant WT-(resCIP4-WT) or ΔP-CIP4 (resCIP4-ΔP) mutants. Left panels: still images of lentivirally infected MCF10A cells induced to scatter by adding EGF are shown. Scale bar represents 100 μm. Right panels: CIP-WT and CIP4-ΔP were detected by IB with the indicated abs. Cell scattering, quantified as in Figures 1G and 1H, is the percentage of accumulated scattering cell distance with respect to the distance of control cells (n = 55 cells per experiment in three experiments). Error bars indicate mean ± SEM. **p < 0.01, compared to scr-CTR MCF10A cells, t test.
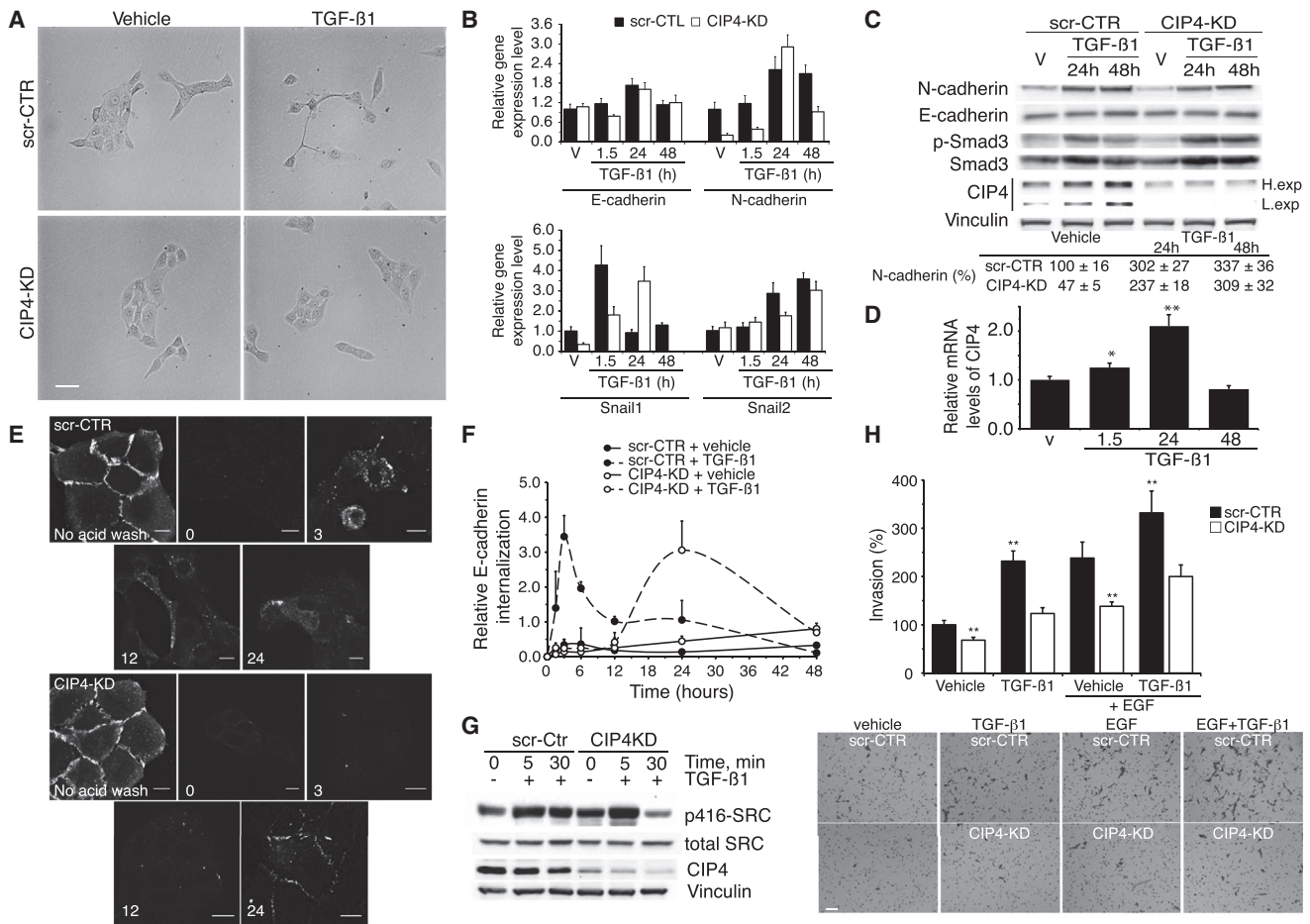
See also Movie S6.

Figure 6. CIP4 Facilitates TGF-β1-Induced Mesenchymal Morphological Conversion in MCF10A Cells

(A) Phase contrast images of scr-CTR and CIP4-KD#1 MCF10A cells treated with 5 ng/ml TGF-β1 or vehicle for 24 hr.

(B) Quantitative RT-PCR of the mRNA of indicated genes from scr-CTR and CIP4-KD MCF10A cells treated with TGF-β1 or vehicle (V). Data are the fold-increase with respect to vehicle treatment (1.5 hr) for each cell sublines normalized for the 18S mRNA levels. h, hr.

(C) Lysates of scr-CTR and CIP4-KD MCF10A cells treated with TGF-β1 (5 ng/ml) or vehicle (V) were subjected to IB with the indicated antibodies. The relative intensity of the N-cadherin with respect to vehicle-treated scr-CTR cells was quantified from three experiments. High exposure (H.exp) and low exposure (L.exp) of CIP4 IB are indicated.

(D) Total RNA was extracted from control MCF10A cells treated with TGF-β1 or vehicle, and CIP4 gene expression was measured by quantitative RT-PCR as described previously.

(E) Internalization of surface-labeled E-cadherin using an anti-E-cadherin (HECD-1) antibody.

(F) Relative levels of internalized E-cadherin were quantified by evaluating total fluorescence intensity and normalized with respect to cell number and field area (in square microns).

(G) Total cell lysates of scr-CTR and CIP4-KD MCF10A cells treated with TGF-β1 (5 ng/ml) or vehicle (V) for the indicated time were subjected to IB with the indicated antibodies.

(H) Invasion assay of scr-CTR and CIP4-KD MCF10A cells pretreated with TGF-β1 (5 ng/ml) or vehicle for 24 hr, done as described in Figure 1I. Cell invasion is the percentage of invasive cells with respect to control cells. *p < 0.05; **p < 0.01 (compared to scr-CTR MCF10A cells pretreated with vehicle), t test. Images of invaded cells are shown. Scale bar represents 100 μm.

Error bars indicate mean ± SEM.

model systems of BC invasion. CIP4 levels are elevated in aggressive ERBB2-positive tumors. Thus, we generated stable CIP4-KD MCF10A cells expressing inducible ERBB2 (MCA-F10A.ERBB2; Muthuswamy et al., 2001). Removal of CIP4 did not affect ERBB2 levels or activation; rather, it slightly increased ERBB2 phosphorylation after stimulation with the dimerizer AP1510 (Figure 8A). However, CIP4 removal diminished Matrigel invasion by more than 3-fold in response to ERBB2 activation (Figure S8A).

Next, we tested the effect of CIP4 depletion on invasion of MCF10A.ERBB2 cells using 3D basement using membrane overlay assays. Untreated MCF10A.ERBB2 cells formed acini with disrupted (multiacinar) morphology (Figure 8B). Following activation of either ERBB2 or TGF-β1 receptors, MCF10A.ERBB2 cells extended rare and poorly invasive protrusions, which became more frequent and highly invasive on concomitant stimulation of both receptors (Figure 8B). Removal of CIP4 robustly prevented the formation of protrusions in
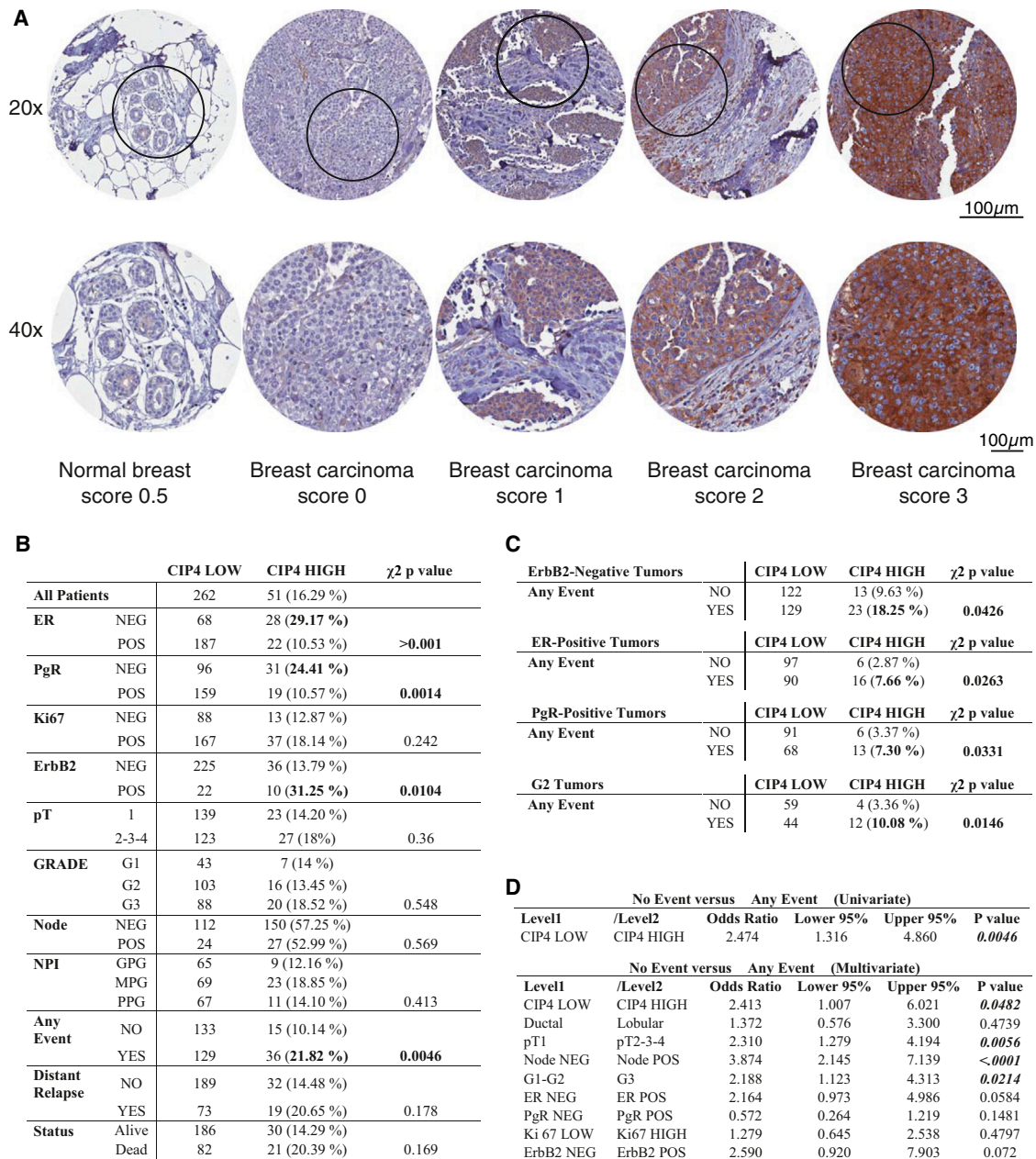
A

20x

40x

100μm

100μm

Normal breast score 0.5 — Breast carcinoma score 0 — Breast carcinoma score 1 — Breast carcinoma score 2 — Breast carcinoma score 3

B

		CIP4 LOW	CIP4 HIGH	χ2 p value
All Patients		262	51 (16.29 %)	
ER	NEG	68	28 (**29.17 %**)	
	POS	187	22 (10.53 %)	>0.001
PgR	NEG	96	31 (**24.41 %**)	
	POS	159	19 (10.57 %)	0.0014
Ki67	NEG	88	13 (12.87 %)	
	POS	167	37 (18.14 %)	0.242
ErbB2	NEG	225	36 (13.79 %)	
	POS	22	10 (**31.25 %**)	0.0104
pT	1	139	23 (14.20 %)	
	2-3-4	123	27 (18%)	0.36
GRADE	G1	43	7 (14 %)	
	G2	103	16 (13.45 %)	
	G3	88	20 (18.52 %)	0.548
Node	NEG	112	150 (57.25 %)	
	POS	24	27 (52.99 %)	0.569
NPI	GPG	65	9 (12.16 %)	
	MPG	69	23 (18.85 %)	
	PPG	67	11 (14.10 %)	0.413
Any Event	NO	133	15 (10.14 %)	
	YES	129	36 (**21.82 %**)	0.0046
Distant Relapse	NO	189	32 (14.48 %)	
	YES	73	19 (20.65 %)	0.178
Status	Alive	186	30 (14.29 %)	
	Dead	82	21 (20.39 %)	0.169

C

ErbB2-Negative Tumors		CIP4 LOW	CIP4 HIGH	χ2 p value
Any Event	NO	122	13 (9.63 %)	
	YES	129	23 (**18.25 %**)	0.0426

ER-Positive Tumors		CIP4 LOW	CIP4 HIGH	χ2 p value
Any Event	NO	97	6 (2.87 %)	
	YES	90	16 (**7.66 %**)	0.0263

PgR-Positive Tumors		CIP4 LOW	CIP4 HIGH	χ2 p value
Any Event	NO	91	6 (3.37 %)	
	YES	68	13 (**7.30 %**)	0.0331

G2 Tumors		CIP4 LOW	CIP4 HIGH	χ2 p value
Any Event	NO	59	4 (3.36 %)	
	YES	44	12 (**10.08 %**)	0.0146

D

No Event versus Any Event	(Univariate)			
Level1	/Level2	Odds Ratio	Lower 95%	Upper 95%	P value
CIP4 LOW	CIP4 HIGH	2.474	1.316	4.860	*0.0046*

No Event versus Any Event	(Multivariate)			
Level1	/Level2	Odds Ratio	Lower 95%	Upper 95%	P value
CIP4 LOW	CIP4 HIGH	2.413	1.007	6.021	*0.0482*
Ductal	Lobular	1.372	0.576	3.300	0.4739
pT1	pT2-3-4	2.310	1.279	4.194	*0.0056*
Node NEG	Node POS	3.874	2.145	7.139	*<0001*
G1-G2	G3	2.188	1.123	4.313	*0.0214*
ER NEG	ER POS	2.164	0.973	4.986	0.0584
PgR NEG	PgR POS	0.572	0.264	1.219	0.1481
Ki 67 LOW	Ki67 HIGH	1.279	0.645	2.538	0.4797
ErbB2 NEG	ErbB2 POS	2.590	0.920	7.903	0.072

Figure 7. Deregulation of CIP4 in Human BC

(A) CIP4 expression was measured by IHC on TMA. Example of CIP4 score assignment: CIP4 high expression was defined when tumors display an expression score >1. In tumor tissues, the IHC signals were associated with the tumor cell and not with the stroma.

(B and C) Correlation of CIP4 expression with clinicopathological parameters. The number of scored cases is lower than the total number of cases (349) since (1) in some cases, individual cores detached from the slides during the manipulations and (2) clinical information was not available for all patients. G2, grade 2.

(D) CIP4 overexpression is predictive of high risk of any breast-related event. Any Event, locoregional relapse, distant metastasis, contralateral BC, or death for BC; Distant Relapse, distant metastasis.

single-agent-treated cells and severely reduced invasive growth of activated MCF10A.ERBB2 in the presence of TGF-β1. In the absence of stimuli, CIP4 depletion had no obvious effects on acini formation and morphology or growth rates (Figure 8B; data not shown). We also stably silenced CIP4 in HCC-1954 cells, which are poorly differentiated, highly metastatic ERBB2-positive BC cells (Gazdar et al., 1998) that display elevated

endogenous levels of CIP4 (Figure S8B). Removal of CIP4 in these cells increased cell compaction (Figures S8C and S8D) and reduced cell invasion (Figure S8E).

Finally, we investigated whether CIP4 is required for the initial local dissemination, invasion, and conversion from a DCIS to IDC. To this end, we stably removed CIP4 in an MCF10A cell derivative, MCFA10.DCIS.com (Figure 8C). These cells have been
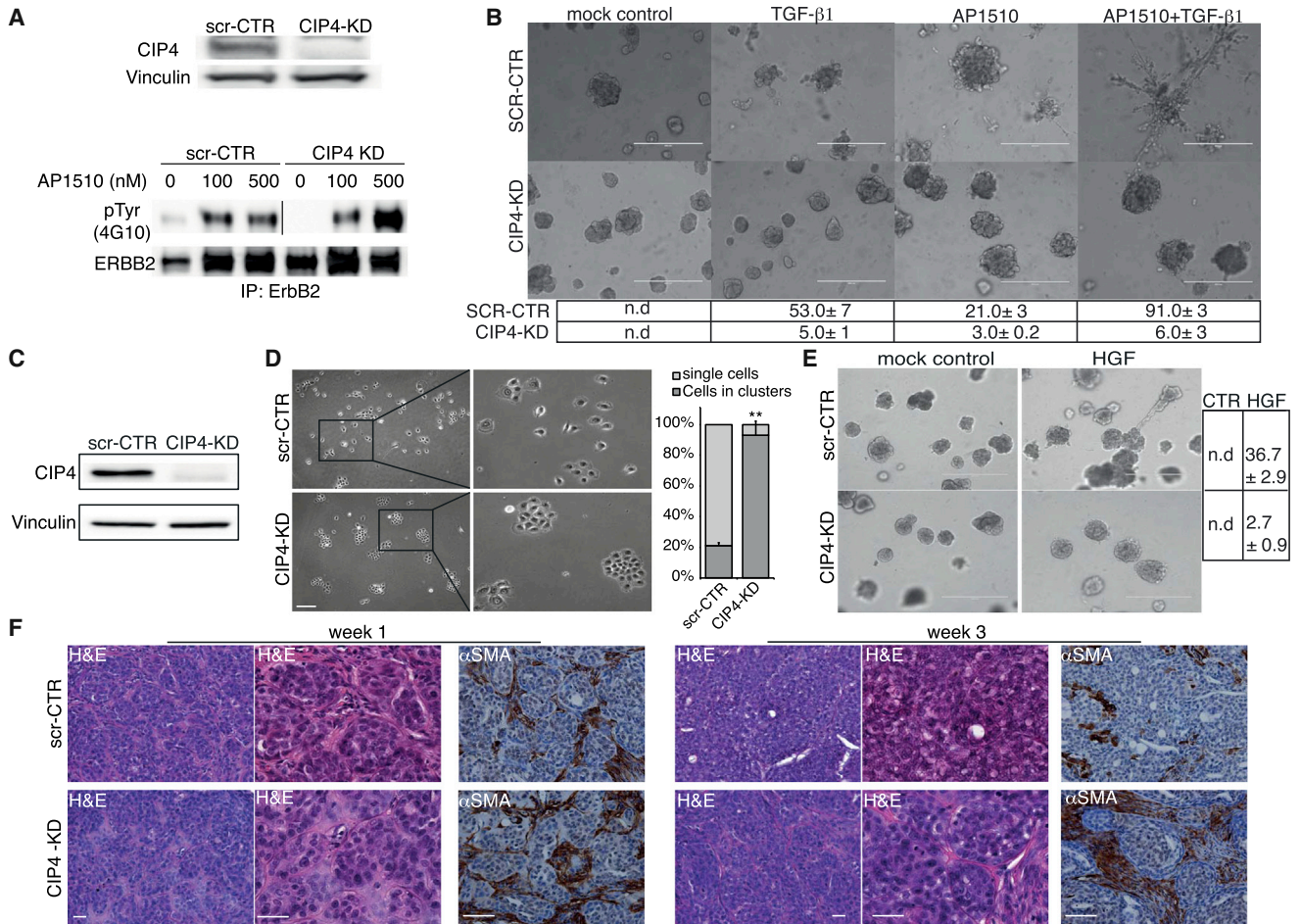
Figure 8. CIP4 Is Required for ERBB2-Induced Invasive Outgrowth in Mammary Epithelial Cells and DCIS-to-IDC Conversion In Vivo
(A) Lysates of lentivirally infected scr-CTR or CIP4-KD#2 MCF10A.ERBB2 cells were immunoblotted with the indicated antibodies. ERBB2 immunoprecipitates (IPs) were immunoblotted with anti-tyrosine antibodies.
(B) Phase contrast micrograph of 7-day acinar structures of scr-CTR and CIP4-KD MCF10A.ERBB2 cells in the presence of TGF-β1 (5 ng/ml), AP1510 (100 nM), or both TGF-β1 (5 ng/ml) and AP1510 (100 nM). Scale bars represent 400 μm. The number of invasive acini is expressed as percentage of total acini ± SEM. (n = 30, three experiments). n.d., not determined.
(C) Lentivirally infected scr-CTR or CIP4-KD#2 MCF10.DCIS.com cells were subjected to IB with the indicated antibodies.
(D) An equal number of scr-CTR and CIP4-KD0MCF10.DCIS.com cells were plated sparsely in complete medium. Phase contrast images are shown. Right panels show a magnified view of the boxed areas shown in left panels. Scale bar represents 250 μm. The percentage of single cells or clusters relative to the total number of MCF10.DCIS.com cells was quantified by counting at least 300 cells per genotype in three independent experiments. **p < 0.01, compared to scr-CTR cells in clusters, t test. Error bars indicate mean ± SEM.
(E) Phase contrast micrograph of 9-day acinar structures of scr-CTR and CIP4-KD MCF.DCIS.com cells in the absence or presence of HGF (20 ng/ml). Scale bars represent 400 μm. Quantification of invasive structures per cell acini is expressed as a percentage of total acini (n = 52 in two independent experiments).
(F) scr-CTR and CIP4-KD MCF10.DCIS.com cells were injected subcutaneously into NSG mice. Histological (hematoxylin and eosin; H&E) and immunohistochemical analyses of scr-CTR and CIP4-KD MCF10.DCIS.com xenografts were performed at 1 and 3 weeks after cell injection. H&E micrographs are shown at two different magnifications. The loss of αSMA-positive myoepithelial layers in control xenograft indicates DCIS-to-IDC conversion. Representative images of three experiments, where n = 5 mice per experimental condition. Scale bars represent 100 μm.

characterized as an experimental model of human DCIS, which forms comedo DCIS-like lesions that spontaneously progress to IDC (Hu et al., 2008; Miller et al., 2000). Depletion of CIP4 in these cells had no effect on cell growth (data not shown) but promoted cell compaction (Figure 8D), impaired hepatocyte growth factor (HGF)-induced invasive outgrowth into a 3D basement membrane matrix (Figure 8E), and severely delayed the DCIS-to-IDC conversion in immunocompromised mice

(Figure 8F). Indeed, MCFA10.DCIS.com control cells formed a typical in situ carcinoma surrounded by a layer of alpha smooth muscle actin (αSMA)-positive myoepithelial cells that, however, was lost 3 weeks after injection, indicative of the acquisition of a highly invasive phenotype (Figure 8F). Depletion of CIP4 impaired this DCIS-to-IDC conversion (Figure 8F). Thus, CIP4 is required for invasion of ERBB2-positive BC, and its removal delays DCIS-to-IDC conversion.

DISCUSSION

Our findings unveil a specific, nonredundant role of the TOCA family member, CIP4, in the regulation of cell-cell junction stability and cell-ECM adhesion during mammalian epithelial morphogenetic events. Endocytosis is a coordinated, spatiotemporal process that requires deformation of the plasma membrane. Through their SH3 and F-BAR domains, members of the TOCA family have the potential to act in a diverse range of internalization processes. Indeed, all the members of this family have been shown to promote actin assembly and to regulate CME, in a redundant fashion, in different model systems (Fricke et al., 2009; Giuliani et al., 2009; Ho et al., 2004). However, there is growing evidence for unique functions of individual TOCA family members. For example, using CIP4 knockout mice, a recent study revealed a unique role of CIP4 in macropinocytosis, indicating that CIP4 is not restricted to CME but also affects other modes of endocytosis (Feng et al., 2010). In addition, roles of CIP4 in cell migration have recently been described in neuronal (Saengsawang et al., 2012) and B lymphoma cells (Malet-Engra et al., 2013). CIP4 has also been shown to regulate the formation of podosomes in primary macrophages (Linder et al., 2000) and invadosomes in breast tumor cells (Hu et al., 2011; Pichot et al., 2010). Together, these studies point to a critical role of CIP4 as a regulator of cell invasion. Our findings support, in part, this notion by establishing that CIP4 controls migration of epithelial cells indirectly by modulating cell cohesion through its "canonical" endocytic function rather than by impairing migratory parameters. This endocytic role is uniquely exerted by CIP4 and not by the other TOCA family members, despite their involvement in CME (Itoh et al., 2005; Wu et al., 2010), indicating that the type of cargo being internalized likely determines functional specificity. It is noteworthy that we found that EGF stimulation promotes the relocalization of CIP4 to E-cadherin junctions, where internalization of this latter protein is initiated. We also observed that EGF causes the relocalization of the protein to extending lamellipodia and ruffles along the protrusive leading edges. Hence, CIP4 might be critical to coordinate junction disassembly, through endocytosis, with the formation of migratory protrusions, ultimately enhancing motility and cell invasion. This latter contention is consistent with our observation that the expression of CIP4, but not TOCA-1 or FBP17, is increased in invasive BC cell lines in comparison with weakly or noninvasive BC cell lines (Hu et al., 2011; Pichot et al., 2010).

Several mechanisms that regulate the availability of E-cadherin for the formation of cell-cell junctions have been proposed. A focal event is the endocytosis and sorting of internalized E-cadherin to either degradation or recycling pathways (Baum nd Georgiou, 2011). In this respect, Rho family GTPases—and most notably, CDC42—regulate not only the formation of AJs but also their dynamic remodeling during tissue rearrangement by controlling multiple steps of E-cadherin trafficking (Harris and Tepass, 2008). In the neuroectodermal epithelium of *Drosophila*, for example, CDC42 and PAR proteins were shown to regulate the trafficking of AJ components and apical polarity proteins to maintain AJ stability in the face of cell rearrangements (Harris and Tepass, 2008). In this system, CDC42, together with the PAR complex, is required to decrease the endocytic uptake

of apical proteins and to promote the progression of apical cargo from the early to the late endosome. Conversely, in the developing pupal notum or dorsal thorax of the fly, CDC42 functions with PAR6/aPKC and CIP4/N-WASP to regulate early events in E-cadherin endocytosis (Georgiou et al., 2008; Leibfried et al., 2008). Therefore, in most epithelial tissues of the fly, the apical polarity complex CDC42–PAR6–aPKC seems to induce the local activation of TOCA family proteins to drive endocytosis of AJ material and the recycling of E-cadherin complexes. In mammary epithelial cells, however, CIP4 is fully dispensable in mediating the activation of a CDC42/N-WASP, a function likely fulfilled by the other members of the family. CIP4 is, instead, essential for the formation of a macromolecular complex that includes E-cadherin and SRC. SRC is a central regulator of signaling downstream of EGFR and has been shown to regulate EMT by disrupting AJs (Canel et al., 2013). Mechanistically, SRC can alter E-cadherin trafficking by redirecting E-cadherin from a recycling pathway to a lysosomal-targeting pathway. This rerouting can be achieved by direct, SRC-mediated tyrosine phosphorylation of E-cadherin cytoplasmic tails, which marks E-cadherin for ubiquitination and subsequent delivery to lysosomal degradation (Fujita et al., 2002). However, we showed that CIP4 removal, despite diminishing EGF-induced activation of SRC and its association with E-cadherin, does not affect E-cadherin phosphorylation (data not shown) or its rate of degradation, suggesting that CIP4 is not essential for this late trafficking step. CIP4 may, instead, act during the early events of endocytosis, where its ability to curve the plasma membrane might facilitate the invagination of newly formed, presumably clathrin-coated, pits. How SRC fits into this scenario remains, however, to be firmly established. One pathway that is activated downstream of SRC involves ROCK kinase and leads to the regulation of actomyosin-dependent junctional contractility (Andreeva et al., 2014), Furthermore, evidence is accumulating of tight interplay between actomyosin contractility and E-cadherin endocytosis during epithelial morphogenesis (Levayer et al., 2011). Within this context, CIP4 may serve as a key molecular hub in interconnecting the two processes, which ultimately affect epithelial cell cohesion, motility, and invasion.

In summary, while further work is required to address the precise molecular mechanisms underlying CIP4 function in cell:ECM adhesion, our data establish the relevance of this endocytic F-BAR-containing protein in mediating, through regulation of cell cohesion, epithelial cell motility and invasive ability. It is therefore not surprising that CIP4 elevation is associated with increased disease relapse of ERBB2-positive BC. In this setting, high levels of CIP4 may have been selected to reduce cell cohesion and cell-cell interaction and promote dissemination. Remarkably, this prometastatic role of CIP4 is not limited to this subset of BC, pointing to a key and essential role of this F-BAR protein in the regulation of BC metastasis.

EXPERIMENTAL PROCEDURES

Cell Motility and Adhesion Assays

Random migration of MCF10A cells was monitored under normal growth conditions. Briefly, cells were seeded (1×10^4 cells per well) in a six-well plate and maintained in complete medium for 2 days. Cell motility was monitored at $37°C$ over a 24 hr period. Pictures were taken every 15 min from 20 positions using an Olympus ScanR system with a Hamamatsu ER camera. Cell tracking was

performed using the Manual Tracking Tool and the Chemotaxis and Migration Tool ImageJ software plug-ins.

For EGF-induced MCF10A cell scattering, cells (1×10^5 cells per well in a six-well plate) were EGF starved for 24 hr and stimulated with 100 ng/ml EGF. Scattering was monitored for 24 hr.

Cell attachment to the substrate was measured using the xCELLigence system (Roche). Briefly, a 96-well plate with microelectronic sensors was coated with 100 μg/ml poly-D-lysine, 10 μg/ml Fn, 5 μg/ml vitronectin, or 10 μg/ml laminin at 4°C and incubated 1 hr with heat-inactivated 5% BSA prior to seeding cells.

Statistical Analysis

For cell biology: differences between experimental groups were examined for statistical significance using the paired Student's t test ($*p < 0.05$, $**p < 0.01$, and $***p < 0.001$). Data are expressed as mean ± SEM.

For TMA tumor sections: differences between experimental groups were examined for statistical significance using paired Student's t test. Where applicable, data are expressed as average ± SEM. TMA data analysis was performed using JMP 10.0 statistical software (SAS Institute). Association between CIP4 expression and clinicopathological parameters was evaluated using Pearson chi-square test. For univariate and multivariate analyses, odds ratio and 95% confidence intervals were obtained from the logistic regression model.

MTT Proliferation Assay

Cells were seeded at 1×10^3 cells per well in 96-well plates and cultured for 36 hr in complete medium before being washed with PBS, and 500 μg/ml MTT [3-(4,5-dimethylthiazol-2-yl)-2,5-diphenyltetrazolium bromide; Sigma-Aldrich] was added to each well. After 2 hr of incubation at 37°C, the MTT solution was removed and 100 μl of DMSO was added to each well. Absorbance was measured at 570 nm using a VICTOR3 V Multilabel Counter (PerkinElmer model 1420).

E-cadherin Internalization

scr-CTR and CIP4-KD MCF10A cells were transfected with human E-cadherin-GFP using Amaxa Nucleofector (Lonza) and seeded (1×10^5) in WillCo-dish glass-bottomed 22-mm-diameter dishes. After 24 hr, cells were EGF starved for a further 24 hr before stimulating with 100 ng/ml EGF. E-cadherin-GFP internalization was then monitored for 4 hr at 37°C. Fluorescence microscopy was performed on an UltraVIEW VoX (PerkinElmer) spinning disk confocal unit, equipped with an EclipseTi inverted microscope (Nikon) and a C9100-50 emCCD camera (Hamamatsu), and driven by Volocity software (Improvision, PerkinElmer). GFP signals and differential interference contrast images were acquired with a 60× oil immersion objective (NA, 1.4) as z stacks (0.7 μm step).

For HECD-1 anti-E-cadherin internalization, cells were grown on glass coverslips and EGF starved for 24 hr before experiments, which were performed as described elsewhere (Paterson et al., 2003). Additional details are in the Supplemental Experimental Procedures.

Surface Biotinylation Assays

The cell surface was labeled for 30 min on ice with 0.5 mg/ml biotin (EZ-Link Sulfo-NH-SS-Biotin) in PBS, pH 7.4. After quenching with 0.15% glycine in PBS, pH 7.4, for 5 min, cells were incubated in complete growth medium supplemented with 100 ng/ml EGF at 37°C for 2 hr. At different time points, cells were removed from the incubator, put on ice, washed with cold MESNA buffer (150 mM NaCl, 1 mM EDTA, 0.2% BSA, 20 mM Tris-HCl, pH 8.6, 50 mM MESNA) to remove cell surface biotin, and lysed. For surface E-cadherin level determination, labeled cells were directly lysed after the quenching step (designated as M). As a negative control (−), cells were directly treated with MESNA buffer after the quenching step without incubation at 37°C. Biotin-labeled proteins were then precipitated using streptavidin-agarose beads and subjected to immunoblotting (IB) with the anti-E-cadherin antibody. Actin levels were used to normalize input protein amounts between different conditions and cell lines.

Internalization and Recycling Assays

^{125}I-EGF surface level, internalization, and recycling assays were performed exactly as described elsewhere (Sorkin and Duex, 2010).

Internalization of total and active β1 integrin was assessed as in Roberts et al. (2001).

Additional details are in the Supplemental Experimental Procedures.

FRET Microscopy and Analysis

EGF-deprived scr-CTR and CIP4-KD MCF10A cells microinjected with either EcadTSModWT or EcadTSModΔCyto constructs were stimulated with EGF (100 ng/ml) to induce scattering. FRET imaging was performed on a Delta Vision Elite system (Applied Precision) equipped with a Photometrics CoolSNAP HQ2 CCD camera and an UPLSApo 60× (NA, 1.42) oil immersion objective (Olympus). The system is coupled with an environmental chamber maintained at 37°C in an atmosphere of 5% CO_2. To monitor the biosensor FRET changes, a ratiometric approach was used as described elsewhere (Aoki and Matsuda, 2009) (see Supplemental Experimental Procedures for details).

Wound Healing Assays

MCF10A scr-CTR and CIP4-KD cells were seeded at 5×10^5 cells per well in six-well plates and cultured until a uniform monolayer had formed. The wound area was made using a pipette tip and washed with PBS. The closure of the wound was then monitored by time-lapse analysis over a 24 hr period, with pictures taken every 5 min. Images were taken with an inverted microscope Olympus ScanR using the 10× objective. The cell-free area was calculated using ImageJ software.

Flow Cytometric Analysis

Expression of the integrins at the cell surface was analyzed by flow cytometry as follows. Briefly, 5×10^5 were incubated with mouse anti-integrin α5β1 or β1 for 1 hr on ice and then incubated with the secondary antibody for 1 hr on ice. After the incubation, cells were fixed with 4% paraformaldehyde for 10 min on ice. Fluorescence-activated cell sorting data were acquired with the FACS-Canto (Becton Dickinson) flow cytometer. Analysis was performed using FlowJo version 4.6.2 (Treestar).

3D Morphogenesis of Mammary Epithelial Cells

The 3D morphogenesis assay was performed as described previously (Debnath et al., 2003).

DCIS-to-IDC Conversion in Nonobese Diabetic/Severe Combined Immunodeficiency Gamma Mice

All animal experiments were performed in accordance with national and international laws and policies. Mice were bred and housed under pathogen-free conditions in our animal facilities at the Cogentech Consortium at the FIRC Institute of Molecular Oncology Foundation and at the European Institute of Oncology in Milan.

Scr-CTR and CIP4-KD MCF10.DCIS.com (100,000 cells) were injected subcutaneously into 6- to 9-week-old female NOD.Cg-Prkdc[scid]Il2rg[tm1Wjl]/SzJ mice—commonly known as nonobese diabetic/severe combined immunodeficiency (NOD SCID) gamma (NSG) mice—in 50% Matrigel (BD Biosciences) as described elsewhere (Hu et al., 2008). One to 3 weeks later, xenografts were measured using digital calipers, and tumor volume was calculated according to the formula $L \times W^2/2 = mm^3$. The tumors were excised, fixed in 4% phosphate-buffered formalin, and embedded in paraffin for IHC staining. The Scan Scope XT device and the Aperio Digital pathology system software (Aperio) were used to capture IHC images.

SUPPLEMENTAL INFORMATION

Supplemental Information includes Supplemental Experimental Procedures, eight figures, and six movies and can be found with this article online at http://dx.doi.org/10.1016/j.devcel.2014.08.006.

AUTHOR CONTRIBUTIONS

Y.R. and P.M. designed, executed, interpreted, and supervised all experiments; C.M. performed 3D invasion assays with ERBB2-positive cells. S.C., C.L., and P.P.D.F. performed and analyzed TMA data on human BC. N.D. and L.L. performed, analyzed, and interpreted integrin internalization assays;

REFERENCES

Andreeva, A., Lee, J., Lohia, M., Wu, X., Macara, I.G., and Lu, X. (2014). PTK7-Src signaling at epithelial cell contacts mediates spatial organization of actomyosin and planar cell polarity. Dev. Cell *29*, 20–33.

Aoki, K., and Matsuda, M. (2009). Visualization of small GTPase activity with fluorescence resonance energy transfer-based biosensors. Nat. Protoc. *4*, 1623–1631.

Aspenström, P. (2009). Roles of F-BAR/PCH proteins in the regulation of membrane dynamics and actin reorganization. Int. Rev. Cell Mol. Biol. *272*, 1–31.

Avizienyte, E., Wyke, A.W., Jones, R.J., McLean, G.W., Westhoff, M.A., Brunton, V.G., and Frame, M.C. (2002). Src-induced de-regulation of E-cadherin in colon cancer cells requires integrin signalling. Nat. Cell Biol. *4*, 632–638.

Baum, B., and Georgiou, M. (2011). Dynamics of adherens junctions in epithelial establishment, maintenance, and remodeling. J. Cell Biol. *192*, 907–917.

Borghi, N., Sorokina, M., Shcherbakova, O.G., Weis, W.I., Pruitt, B.L., Nelson, W.J., and Dunn, A.R. (2012). E-cadherin is under constitutive actomyosin-generated tension that is increased at cell-cell contacts upon externally applied stretch. Proc. Natl. Acad. Sci. USA *109*, 12568–12573.

Bresnick, A.R. (1999). Molecular mechanisms of nonmuscle myosin-II regulation. Curr. Opin. Cell Biol. *11*, 26–33.

Canel, M., Serrels, A., Miller, D., Timpson, P., Serrels, B., Frame, M.C., and Brunton, V.G. (2010). Quantitative in vivo imaging of the effects of inhibiting integrin signaling via Src and FAK on cancer cell movement: effects on E-cadherin dynamics. Cancer Res. *70*, 9413–9422.

Canel, M., Serrels, A., Frame, M.C., and Brunton, V.G. (2013). E-cadherin-integrin crosstalk in cancer invasion and metastasis. J. Cell Sci. *126*, 393–401.

de Rooij, J., Kerstens, A., Danuser, G., Schwartz, M.A., and Waterman-Storer, C.M. (2005). Integrin-dependent actomyosin contraction regulates epithelial cell scattering. J. Cell Biol. *171*, 153–164.

Debnath, J., Muthuswamy, S.K., and Brugge, J.S. (2003). Morphogenesis and oncogenesis of MCF-10A mammary epithelial acini grown in three-dimensional basement membrane cultures. Methods *30*, 256–268.

Dombrosky-Ferlan, P., Grishin, A., Botelho, R.J., Sampson, M., Wang, L., Rudert, W.A., Grinstein, S., and Corey, S.J. (2003). Felic (CIP4b), a novel binding partner with the Src kinase Lyn and Cdc42, localizes to the phagocytic cup. Blood *101*, 2804–2809.

Feng, Y., Hartig, S.M., Bechill, J.E., Blanchard, E.G., Caudell, E., and Corey, S.J. (2010). The Cdc42-interacting protein-4 (CIP4) gene knock-out mouse reveals delayed and decreased endocytosis. J. Biol. Chem. *285*, 4348–4354.

Fricke, R., Gohl, C., Dharmalingam, E., Grevelhörster, A., Zahedi, B., Harden, N., Kessels, M., Qualmann, B., and Bogdan, S. (2009). Drosophila Cip4/Toca-1 integrates membrane trafficking and actin dynamics through WASP and SCAR/WAVE. Curr. Biol. *19*, 1429–1437.

Fujita, Y., Krause, G., Scheffner, M., Zechner, D., Leddy, H.E., Behrens, J., Sommer, T., and Birchmeier, W. (2002). Hakai, a c-Cbl-like protein, ubiquitinates and induces endocytosis of the E-cadherin complex. Nat. Cell Biol. *4*, 222–231.

Gazdar, A.F., Kurvari, V., Virmani, A., Gollahon, L., Sakaguchi, M., Westerfield, M., Kodagoda, D., Stasny, V., Cunningham, H.T., Wistuba, I.I., et al. (1998). Characterization of paired tumor and non-tumor cell lines established from patients with breast cancer. Int. J. Cancer *78*, 766–774.

Geiger, B., Spatz, J.P., and Bershadsky, A.D. (2009). Environmental sensing through focal adhesions. Nat. Rev. Mol. Cell Biol. *10*, 21–33.

Georgiou, M., Marinari, E., Burden, J., and Baum, B. (2008). Cdc42, Par6, and aPKC regulate Arp2/3-mediated endocytosis to control local adherens junction stability. Curr. Biol. *18*, 1631–1638.

Giuliani, C., Troglio, F., Bai, Z., Patel, F.B., Zucconi, A., Malabarba, M.G., Disanza, A., Stradal, T.B., Cassata, G., Confalonieri, S., et al. (2009). Requirements for F-BAR proteins TOCA-1 and TOCA-2 in actin dynamics and membrane trafficking during Caenorhabditis elegans oocyte growth and embryonic epidermal morphogenesis. PLoS Genet. *5*, e1000675.

Harris, K.P., and Tepass, U. (2008). Cdc42 and Par proteins stabilize dynamic adherens junctions in the Drosophila neuroectoderm through regulation of apical endocytosis. J. Cell Biol. *183*, 1129–1143.

Ho, H.Y., Rohatgi, R., Lebensohn, A.M., Le Ma, Li, J., Gygi, S.P., and Kirschner, M.W. (2004). Toca-1 mediates Cdc42-dependent actin nucleation by activating the N-WASP-WIP complex. Cell *118*, 203–216.

Hu, M., Yao, J., Carroll, D.K., Weremowicz, S., Chen, H., Carrasco, D., Richardson, A., Violette, S., Nikolskaya, T., Nikolsky, Y., et al. (2008). Regulation of in situ to invasive breast carcinoma transition. Cancer Cell *13*, 394–406.

Hu, J., Mukhopadhyay, A., Truesdell, P., Chander, H., Mukhopadhyay, U.K., Mak, A.S., and Craig, A.W. (2011). Cdc42-interacting protein 4 is a Src substrate that regulates invadopodia and invasiveness of breast tumors by promoting MT1-MMP endocytosis. J. Cell Sci. *124*, 1739–1751.

Hyafil, F., Babinet, C., and Jacob, F. (1981). Cell-cell interactions in early embryogenesis: a molecular approach to the role of calcium. Cell *26*, 447–454.

Itoh, T., Erdmann, K.S., Roux, A., Habermann, B., Werner, H., and De Camilli, P. (2005). Dynamin and the actin cytoskeleton cooperatively regulate plasma membrane invagination by BAR and F-BAR proteins. Dev. Cell *9*, 791–804.

Janda, E., Nevolo, M., Lehmann, K., Downward, J., Beug, H., and Grieco, M. (2006). Raf plus TGFbeta-dependent EMT is initiated by endocytosis and lysosomal degradation of E-cadherin. Oncogene *25*, 7117–7130.

le Duc, Q., Shi, Q., Blonk, I., Sonnenberg, A., Wang, N., Leckband, D., and de Rooij, J. (2010). Vinculin potentiates E-cadherin mechanosensing and is recruited to actin-anchored sites within adherens junctions in a myosin II-dependent manner. J. Cell Biol. *189*, 1107–1115.

Leibfried, A., Fricke, R., Morgan, M.J., Bogdan, S., and Bellaiche, Y. (2008). Drosophila Cip4 and WASp define a branch of the Cdc42-Par6-aPKC pathway regulating E-cadherin endocytosis. Curr. Biol. *18*, 1639–1648.

Levayer, R., Pelissier-Monier, A., and Lecuit, T. (2011). Spatial regulation of Dia and Myosin-II by RhoGEF2 controls initiation of E-cadherin endocytosis during epithelial morphogenesis. Nat. Cell Biol. *13*, 529–540.

Linder, S., Hüfner, K., Wintergerst, U., and Aepfelbacher, M. (2000). Microtubule-dependent formation of podosomal adhesion structures in primary human macrophages. J. Cell Sci. *113*, 4165–4176.

Malet-Engra, G., Viaud, J., Ysebaert, L., Farcé, M., Lafouresse, F., Laurent, G., Gaits-Iacovoni, F., Scita, G., and Dupré, L. (2013). CIP4 controls CCL19-driven

cell steering and chemotaxis in chronic lymphocytic leukemia. Cancer Res. *73*, 3412–3424.

Miller, F.R., Santner, S.J., Tait, L., and Dawson, P.J. (2000). MCF10DCIS.com xenograft model of human comedo ductal carcinoma in situ. J. Natl. Cancer Inst. *92*, 1185–1186.

Muthuswamy, S.K., Li, D., Lelievre, S., Bissell, M.J., and Brugge, J.S. (2001). ErbB2, but not ErbB1, reinitiates proliferation and induces luminal repopulation in epithelial acini. Nat. Cell Biol. *3*, 785–792.

Ogata, S., Morokuma, J., Hayata, T., Kolle, G., Niehrs, C., Ueno, N., and Cho, K.W. (2007). TGF-beta signaling-mediated morphogenesis: modulation of cell adhesion via cadherin endocytosis. Genes Dev. *21*, 1817–1831.

Orlichenko, L., Weller, S.G., Cao, H., Krueger, E.W., Awoniyi, M., Beznoussenko, G., Buccione, R., and McNiven, M.A. (2009). Caveolae mediate growth factor-induced disassembly of adherens junctions to support tumor cell dissociation. Mol. Biol. Cell *20*, 4140–4152.

Palacios, F., Tushir, J.S., Fujita, Y., and D'Souza-Schorey, C. (2005). Lysosomal targeting of E-cadherin: a unique mechanism for the down-regulation of cell-cell adhesion during epithelial to mesenchymal transitions. Mol. Cell. Biol. *25*, 389–402.

Paterson, A.D., Parton, R.G., Ferguson, C., Stow, J.L., and Yap, A.S. (2003). Characterization of E-cadherin endocytosis in isolated MCF-7 and chinese hamster ovary cells: the initial fate of unbound E-cadherin. J. Biol. Chem. *278*, 21050–21057.

Peinado, H., Portillo, F., and Cano, A. (2004). Transcriptional regulation of cadherins during development and carcinogenesis. Int. J. Dev. Biol. *48*, 365–375.

Pichot, C.S., Arvanitis, C., Hartig, S.M., Jensen, S.A., Bechill, J., Marzouk, S., Yu, J., Frost, J.A., and Corey, S.J. (2010). Cdc42-interacting protein 4 promotes breast cancer cell invasion and formation of invadopodia through activation of N-WASp. Cancer Res. *70*, 8347–8356.

Qian, X., Karpova, T., Sheppard, A.M., McNally, J., and Lowy, D.R. (2004). E-cadherin-mediated adhesion inhibits ligand-dependent activation of diverse receptor tyrosine kinases. EMBO J. *23*, 1739–1748.

Roberts, M., Barry, S., Woods, A., van der Sluijs, P., and Norman, J. (2001). PDGF-regulated rab4-dependent recycling of alphavbeta3 integrin from early endosomes is necessary for cell adhesion and spreading. Curr. Biol. *11*, 1392–1402.

Saengsawang, W., Mitok, K., Viesselmann, C., Pietila, L., Lumbard, D.C., Corey, S.J., and Dent, E.W. (2012). The F-BAR protein CIP4 inhibits neurite formation by producing lamellipodial protrusions. Curr. Biol. *22*, 494–501.

Shen, Y., Hirsch, D.S., Sasiela, C.A., and Wu, W.J. (2008). Cdc42 regulates E-cadherin ubiquitination and degradation through an epidermal growth factor receptor to Src-mediated pathway. J. Biol. Chem. *283*, 5127–5137.

Sorkin, A., and Duex, J.E. (2010). Quantitative analysis of endocytosis and turnover of epidermal growth factor (EGF) and EGF receptor. Curr. Protoc. Cell Biol. *Chapter 15*, Unit 15.14.

Thiery, J.P., Acloque, H., Huang, R.Y., and Nieto, M.A. (2009). Epithelial-mesenchymal transitions in development and disease. Cell *139*, 871–890.

Tian, L., Nelson, D.L., and Stewart, D.M. (2000). Cdc42-interacting protein 4 mediates binding of the Wiskott-Aldrich syndrome protein to microtubules. J. Biol. Chem. *275*, 7854–7861.

Torres, E., and Rosen, M.K. (2003). Contingent phosphorylation/dephosphorylation provides a mechanism of molecular memory in WASP. Mol. Cell *11*, 1215–1227.

Wu, M., Huang, B., Graham, M., Raimondi, A., Heuser, J.E., Zhuang, X., and De Camilli, P. (2010). Coupling between clathrin-dependent endocytic budding and F-BAR-dependent tubulation in a cell-free system. Nat. Cell Biol. *12*, 902–908.